An Analysis of Cloud Drop Growth by Collection: Part IV. A New Parameterization[1]

EDWIN X BERRY[2]

National Science Foundation, Washington, D. C. 20550

RICHARD L. REINHARDT

Sierra Nevada Corporation, Reno, Nev. 89507

(Manuscript received 29 January 1974, in revised form 23 July 1974)

ABSTRACT

A new parameterization of cloud particle growth combines the effects of accretion and self-collection, and frees the large-hydrometeor water mass and spectral moments to grow independently. The large-hydrometeor water mass grows through accretion in proportion to the cloud water mass. The spectral moments grow through self-collection in proportion to the large-hydrometeor water content. Accretion is also dependent upon the magnitude of the spectral moments and thus an important feedback loop occurs.

The spreading or narrowing of the drop spectrum is dependent upon the collection kernel and the relative magnitudes of accretion and self-collection in the region of interest. These effects are included in the parameterization. In order for the spectrum to spread there must exist both the stochastic mode and a sufficiently rapid increase in the collection kernel with drop size.

1. Introduction

Part I of this series illustrated the strong differences produced in the growth of a droplet spectrum by the accretion and self-collection modes of stochastic collection. The accretion mode, using the continuous approximation of having the larger (collecting) drops a diameter or more larger than the smaller (collected) droplets, produced a growing but narrowing spectrum, while the self-collection mode, drawing upon the interaction among drops more nearly their own size, produced a rapidly spreading spectrum. It was anticipated that the spreading or narrowing was also a result of certain properties of the collection kernel. This paper will analyze the effect of the kernel on each mode of collection.

Part II pointed out regularities associated with the development of several initial spectra. The increase of the predominant radius r_g up to about 50 μm was slower for those spectra with smaller kernels at their points of origin and with stronger initial spreading. Once beyond 50 μm, the rate of change of r_g was essentially the same for all spectra independent of the amount of water mass on the large-hydrometeor portion of the spectrum. Also, all broadened spectra then began to assume similar Golovin-type shapes. This paper will show some mathematical reasons for this behavior.

Part III laid the mathematical basis for the parameterization of the growth of the large-hydrometeor spectrum. It was shown how accretion and self-collection could be treated separately and their effects superimposed through parameterized rate equations with defined rate coefficients. Values of these rate coefficients were calculated and plotted (reproduced here in Fig. 1). These provide the basis for the discussion in this paper of some fundamental features of drop growth by collection.

2. Fundamentals of spectrum spreading

Part III showed the derivation of the four basic equations for the parameterized drop growth, i.e., the growth rates of x_g and x_f for both continuous and stochastic modes. These equations are

$$\frac{1}{x_{g2}}\frac{dx_{g2}}{dt}\bigg|_c = \frac{L_1}{L_2}\int_{S2} V(x_2|x_1)\left(\frac{2x_2}{x_{g2}}-1\right)f\langle x_2\rangle dx_2, \tag{1}$$

$$\frac{1}{x_{f2}}\frac{dx_{f2}}{dt}\bigg|_c = \frac{L_1}{L_2}\int_{S2} V(x_2|x_1)f\langle x_2\rangle dx_2, \tag{2}$$

$$\frac{1}{x_{g2}}\frac{dx_{g2}}{dt}\bigg|_s = \frac{1}{Z_2}\int_{S2} dx\int_{S2} dx'\, xx' f\langle x\rangle V(x|x')f\langle x'\rangle, \tag{3}$$

$$\frac{1}{x_{f2}}\frac{dx_{f2}}{dt}\bigg|_s = \frac{1}{2N_2}\int_{S2} dx\int_{S2} dx'\, f\langle x\rangle V(x|x')f\langle x'\rangle, \tag{4}$$

where the subscript c refers to the continuous or ac-

[1] See Part III for acknowledgments.

[2] Present affiliation: National Science Foundation, Western Projects Office, Burlingame, Calif. 90410.

cretion mode and s to the stochastic or self-collection mode.

Using the three analytic kernels, namely,

$$V_1(x|x')=b_1xx', \tag{5a}$$

$$V_2(x|x')=b_2(x+x'), \tag{5b}$$

$$V_3(x|x')=b_3, \tag{5c}$$

in Eqs. (1)–(4), we derive the growth rates for x_g and x_f under each of the six situations:

$$\frac{1}{x_{g2}}\frac{dx_{g2}}{dt}\bigg|_{c,1}=x_1b_1L_1 \tag{6a}$$

$$\frac{1}{x_{g2}}\frac{dx_{g2}}{dt}\bigg|_{c,2}=\left(1+\frac{2x_1}{x_{g2}}-\frac{x_1}{x_{f2}}\right)b_2L_1 \tag{6b}$$

$$\frac{1}{x_{g2}}\frac{dx_{g2}}{dt}\bigg|_{c,3}=\left(\frac{2}{x_{g2}}-\frac{1}{x_{f2}}\right)b_3L_1 \tag{6c}$$

$$\frac{1}{x_{f2}}\frac{dx_{f2}}{dt}\bigg|_{c,1}=x_1b_1L_1 \tag{7a}$$

$$\frac{1}{x_{f2}}\frac{dx_{f2}}{dt}\bigg|_{c,2}=b_2L_1 \tag{7b}$$

$$\frac{1}{x_{f2}}\frac{dx_{f2}}{dt}\bigg|_{c,3}=\frac{1}{x_{f2}}b_3L_1 \tag{7c}$$

$$\frac{1}{x_{g2}}\frac{dx_{g2}}{dt}\bigg|_{s,1}=x_{g2}b_1L_2 \tag{8a}$$

$$\frac{1}{x_{g2}}\frac{dx_{g2}}{dt}\bigg|_{s,2}=2b_2L_2 \tag{8b}$$

$$\frac{1}{x_{g2}}\frac{dx_{g2}}{dt}\bigg|_{s,3}=\frac{1}{x_{g2}}b_3L_2 \tag{8c}$$

$$\frac{1}{x_{f2}}\frac{dx_{f2}}{dt}\bigg|_{s,1}=\tfrac{1}{2}x_{f2}b_1L_2 \tag{9a}$$

$$\frac{1}{x_{f2}}\frac{dx_{f2}}{dt}\bigg|_{s,2}=b_2L_2 \tag{9b}$$

$$\frac{1}{x_{f2}}\frac{dx_{f2}}{dt}\bigg|_{s,3}=\frac{1}{2}\frac{1}{x_{f2}}b_3L_2. \tag{9c}$$

Excluding the second-order correction proportional to x_1 in (6b), the continuous mode changes x_{g2} and x_{f2} equally for kernels 1 and 2, which are the more important kernels for cloud physics applications. For kernel 3, x_{f2} increases as a function of b_3L_1/x_{f2}, while x_g tracks x_{f2}, decreasing when it is larger than $2x_{f2}$, and growing when it is smaller [(6c)] but not fast enough to prevent x_{f2} from closing in. As x_{f2} approaches x_{g2}, the growth rate of x_{g2} increases until it is the same as that of x_{f2}, forming a delta function, and thereafter the tracking is exact and the delta function cannot spread.

For the stochastic mode the growth rates of x_{f2} are just one-half those for x_{g2} when x_{f2} and x_{g2} are equal. For comparison between kernels 1, 2, 3, we arbitrarily set the growth rates of x_{g2} equal at the boundaries between 1 and 2, and 2 and 3. Therefore,

$$[x_1b_1=b_2=b_3/x_c]_c, \tag{10}$$

$$[x_ab_1=2b_2=b_3/x_c]_s, \tag{11}$$

where x_a and x_c are the lower and upper bounds of region 2, and apply to both x_{f2} and x_{g2}.

We are now in a position to investigate the spectrum spreading due to the stochastic and continuous modes for the three analytic kernels. We distinguish five general ranges of collection depending upon whether x_{g2} and x_{f2} fall into regions 1, 2 or 3, of the analytic kernels, and designate these ranges by the subscripts 11, 21, 22, 32, 33, respectively. Using

$$\frac{d}{dt}(\text{var } x)=\frac{x_g}{x_f}\left(\frac{1}{x_g}\frac{dx_g}{dt}-\frac{1}{x_f}\frac{dx_f}{dt}\right), \tag{12}$$

we evaluate the spreading rate for the five ranges for both continuous and stochastic modes:

$$\frac{d}{dt}(\text{var } x)_{c,11}=0 \tag{13a}$$

$$\frac{d}{dt}(\text{var } x)_{c,21}=\frac{x_{g2}}{x_{f2}}\left(\frac{2}{x_{g2}}-\frac{1}{x_{f2}}\right)x_1b_2L_1 \tag{13b}$$

$$\frac{d}{dt}(\text{var } x)_{c,22}=\frac{x_{g2}}{x_{f2}}\left(\frac{2}{x_{g2}}-\frac{1}{x_{f2}}\right)x_1b_2L_1 \tag{13c}$$

$$\frac{d}{dt}(\text{var } x)_{c,32}=\frac{x_{g2}}{x_{f2}}\left(\frac{2b_3}{x_{g2}}-\frac{b_3}{x_{f2}}-b_2\right)L_1 \tag{13d}$$

$$\frac{d}{dt}(\text{var } x)_{c,33}=\frac{x_{g2}}{x_{f2}}\left(\frac{1}{x_{g2}}-\frac{1}{x_{f2}}\right)2b_3L_1 \tag{13e}$$

$$\frac{d}{dt}(\text{var } x)_{s,11}=\frac{x_{g2}}{x_{f2}}(x_{g2}-\tfrac{1}{2}x_{f2})b_1L_2 \tag{14a}$$

$$\frac{d}{dt}(\text{var } x)_{s,21}=\frac{x_{g2}}{x_{f2}}(2b_2-\tfrac{1}{2}x_{f2}b_1)L_2 \tag{14b}$$

$$\frac{d}{dt}(\text{var } x)_{s,22}=\frac{x_{g2}}{x_{f2}}(2-1)b_2L_2 \tag{14c}$$

$$\frac{d}{dt}(\text{var } x)_{s,32}=\frac{x_{g2}}{x_{f2}}\left(\frac{b_3}{x_{g2}}-b_2\right)L_2 \tag{14d}$$

$$\frac{d}{dt}(\text{var } x)_{s,33}=\frac{x_{g2}}{x_{f2}}\left(\frac{1}{x_{g2}}-\frac{1}{2x_{f2}}\right)b_3L_2. \tag{14e}$$

Both the growth and spreading for the continuous mode depend upon L_1 while those for the stochastic mode depend upon L_2. For the stochastic mode at constant L_2, these ranges represent successive, gradual slowings of the rate of spreading.

The spreading produced by the continuous mode for kernel 1 is zero while that for kernel 2 produces an approach to var $x=1$, although slowly by virtue of the small coefficient x_1. That for kernel 3 is negative going to zero when the spectrum approaches the delta function ($x_{g2}=x_{f2}$ and var $x=0$) [(13e)]. In the first overlapping range [(13b)] the spreading is the same as for kernel 2. In the second overlapping range [(13d)] the spreading is, by virtue of our discussion of (6c), negative for all but the delta function, for which the spreading is zero.

For the stochastic mode the spreading rate of (14a) is smallest, but non-zero, when $x_{g2}=x_{f2}$ and increases as x_{g2} increases. When x_{g2} enters the second region [(14b)] the spreading rate gradually diminishes as x_{f2} increases until $x_{f2}b_1=2b_2$, as in (11). Then (14c) applies and the spreading rate depends only on the ratio x_{g2}/x_{f2} (assuming L_2 constant). Eventually $2b_2=b_3/x_{g2}$ and growth enters region 4 [(14d)] and the spreading rate gradually decreases. It goes to zero when $x_{g2}=b_3/b_2$, and negative for $x_{g2}>b_3/b_2$ (because x_{f2} continues to increase rapidly while x_{g2} slows down). When $2b_2=b_3/x_f$ (which, incidentally, never happened in the calculations performed) we are already in the area of negative spreading [(14e)]. It continues negative as $2x_{f2}$ closes in on x_{g2} where an equilibrium state is reached.

This latter equilibrium state of (14e) corresponds to var $x=1$ which is the shape found in some initial distributions of Part II. It is a self-preserving form on the $g\langle\ln r\rangle$ plot for the constant kernel. Similarly, (14a) and (14c) are the formulas for the spreading resulting from kernels 1 and 2, respectively, as discussed in Part III. The spreading rate of (14c) also has been shown (Berry, 1967) to produce a self-preserving form on the $g\langle\ln r\rangle$ plot.

These relationships may be observed in yet another way. We define $R_{s,i}$ and $R_{c,i}$ as the ratios of the spreading to the growth rates for each mode and for each analytic kernel, where $i=1, 2, 3$. Thus,

$$R_{s,i}=\frac{\dfrac{d}{dt}(\text{var } x)_{s,ii}}{\dfrac{1}{x_{g2}}\dfrac{dx_{g2}}{dt}\Big|_{s,i}}, \tag{15}$$

and similarly for $R_{c,i}$. Then from the above we have the following:

$$R_{c,1}=0 \tag{16a}$$

$$R_{c,2}=\frac{x_1}{x_{f2}}(1-\text{var } x) \tag{16b}$$

$$R_{c,3}=-2 \text{ var } x(1+\text{var } x)/(1-\text{var } x) \tag{16c}$$

$$R_{s,1}=\tfrac{1}{2}(1+2 \text{ var } x) \tag{17a}$$

$$R_{s,2}=\tfrac{1}{2}(1+\text{var } x) \tag{17b}$$

$$R_{s,3}=\tfrac{1}{2}(1+\text{var } x)(1-\text{var } x). \tag{17c}$$

The greatest relative spreading rate is given by $R_{s,1}$, followed by $R_{s,2}$. $R_{s,3}$ seeks the equilibrium state var $x=1$. The continuous mode shows no spreading for $R_{c,1}$ while $R_{c,2}$ shows a very slow approach to var $x=1$. The numerator of $R_{c,3}$ is the spreading rate, which is always negative until var $x=0$. The denominator of $R_{c,3}$ is the growth rate of x_{g2} which is negative for var $x>1$ and positive for var $x<1$. Thus, if the distribution is very broad (var $x>1$) $R_{c,3}$ shows that x_{g2} decreases in value simultaneously with the decrease in var x. Once var $x<1$, the x_{g2} increases while var x continues to decrease to a delta function.

There is no important spreading produced by the continuous mode. The spectrum variance remains unchanged by this process for kernel 1, goes slowly to 1 for kernel 2 and to the delta function for kernel 3. This is the reason for the narrowing of $S2$ seen in Part I.

The stochastic mode is necessary but not sufficient for spectrum spreading. Given the stochastic mode, spreading is highly dependent upon the rate of increase with x and x' of the collection kernel as shown in (5). When this increase is large as it is for kernel 1 the spreading rate is large [see Eq. (14a)]. When it is moderate, as it is for kernel 2, the spreading rate is also moderate [(14c)]. When it is zero, as it is for kernel 3, the spreading is negative if var $x>1$, positive for var $x<1$, and tends to zero as var x approaches 1 [(14e)].

Thus, any complete explanation of the spreading of $S2$, as shown in Part I must include the effect of the rate of increase of the kernel with droplet size. Were it not for the fact that the kernel increases very rapidly in the region of the $S2$ tail in Fig. 6 (Part I), then indeed such spreading would not occur. Were the kernel in this region roughly $b_2(x+x')$, as it is for the intermediate-sized drops, the $S2$ would not have so lengthened its tail but would rather have grown in the fashion of the intermediate drops, keeping its shape similar to the Golovin asymptotic form.

3. Simultaneous effects of accretion and self-collection

In order to set the parameterized equations in a more usuable form we have defined in Part III spe-

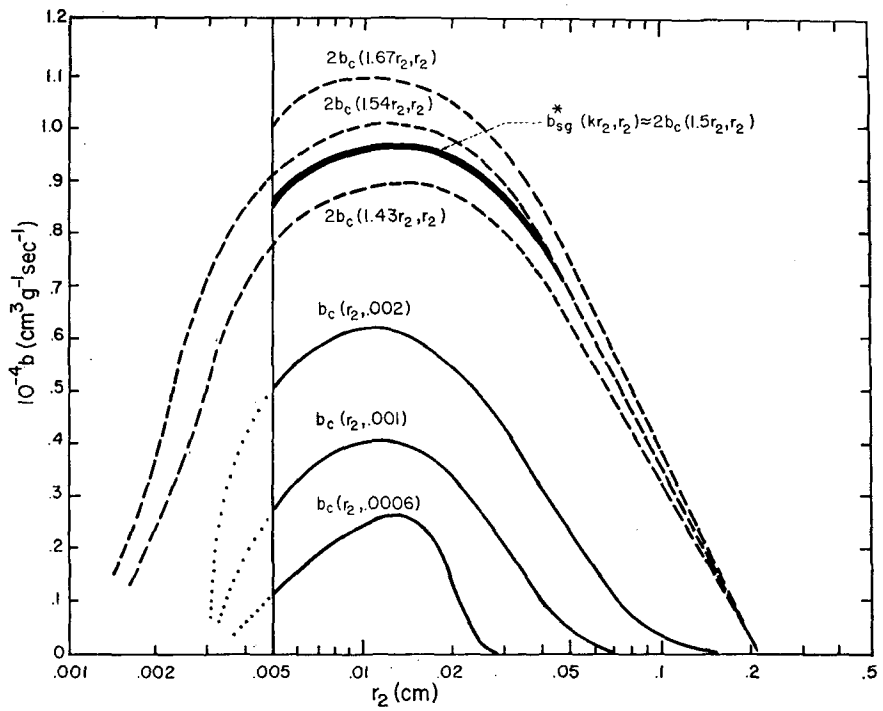

FIG. 1. The values of $b_c(r_2,r_1)$ for the accretion parameterization and $b^*_s(r_{g2})$ for the self-collection parameterization (from Part III).

cialized rate coefficients in terms of the following equations:

$$\frac{1}{x_{g2}}\frac{dx_{g2}}{dt}\bigg|_c \equiv b^*_{cg}(x_{g2},x_1)L_1 \tag{18}$$

$$\frac{1}{x_{f2}}\frac{dx_{f2}}{dt}\bigg|_c \equiv b^*_{cf}(x_{g2},x_1)L_1 \tag{19}$$

$$\frac{1}{x_{g2}}\frac{dx_{g2}}{dt}\bigg|_s \equiv b^*_{sg}(x_{g2})L_2 \tag{20}$$

$$\frac{1}{x_{f2}}\frac{dx_{f2}}{dt}\bigg|_s \equiv b^*_{sf}(x_{g2},x_{f2})L_2. \tag{21}$$

By comparison to (1), (2), (3) and (4) it is evident that these specialized rate coefficients take on the following values:

$$b^*_{cg}(x_{g2},x_1)=\frac{1}{L_2}\int_{S2} V(x_2|x_1)\left(\frac{2x_2}{x_{g2}}-1\right)f\langle x_2\rangle dx_2 \tag{22}$$

$$b^*_{cf}(x_{g2},x_1)=\frac{1}{L_2}\int_{S2} V(x_2|x_1)f\langle x_2\rangle dx_2 \tag{23}$$

$$b^*_{sg}(x_{g2})=\frac{1}{L_2Z_2}\int_{S2} dx\int_{S2} dx'xx'f\langle x\rangle V(x|x')f\langle x'\rangle \tag{24}$$

$$b^*_{sf}(x_{g2},x_{f2})=\frac{1}{2N_2L}\int_{S2} dx\int_{S2} dx'f\langle x\rangle V(x|x')f\langle x'\rangle. \tag{25}$$

The kernel V is conveniently related in Part III to the accretion mode rate coefficient b_c as

$$b_c(x_2,x_1)\equiv V(x_2|x_1)/(x_2+x_1). \tag{26}$$

The values of b_c and b^*_{sg} as calculated in Part III are displayed in Fig. 1.

In the region where b_c is almost a constant, i.e., for $50\ \mu\text{m}\leqslant r_2\leqslant 200\ \mu\text{m}$ and $r_{f1}\geqslant 8\ \mu$m, Eqs. (22) and (23) reduce to the approximations

$$b^*_{cf}(x_{g2},x_1)\approx b_c(x_{g2},x_1), \tag{27}$$

$$b^*_{cg}(x_{g2},x_1)\approx b_c(x_{g2},x_1). \tag{28}$$

Although (24) can be readily reduced to

$$b^*_{sg}(x_{g2})=\frac{2}{L_2Z_2}\int_{S2} x^2f\langle x\rangle dx\int_{S2} b_c(x,x')x'f\langle x'\rangle dx', \tag{29}$$

it is difficult to derive analytically an approximation for b^*_{sg}. However, such an approximation was derived empirically in Part III, as shown in Fig. 1; the result was

$$b^*_{sg}(x_{g2})\approx 2b_c(3.4x_{g2},x_{g2}), \tag{30a}$$

$$b^*_{sg}(r_{g2})\approx 2b_c(1.5r_{g2},r_{g2}). \tag{30b}$$

TABLE 1. Calculations of growth rates of r_g and r_{g2} for Figs. 1–6 of Part II at the moment when $r_g = 50$ μm. The rates are to be compared with curves on Fig. 7 of Part II.

Figure no. (Part II)	r_f (×10⁴)	r_b (×10⁴)	r_{g1} (×10⁴)	r_{g2} (×10⁴)	L_1 (×10⁶)	L_2 (×10⁶)	b_c (×10⁻⁴)	b^*_{sg} (×10⁻⁴)	$L_1 b_c$ (×10²)	$L_2 b^*_{sg}$ (×10²)	$\times\left(\frac{1}{r^3_{g2}}\right)\times\left(\frac{dr^3_{g2}}{dt}\right)$ (×10²)	$\times\left(\frac{1}{r^3_g}\right)\times\left(\frac{dr^3_g}{dt}\right)$ (×10²)
1	10	10	12.5	110	0.91	0.094	0.47	0.97	0.43	0.09	0.52	0.95
2	14	11.1	15.0	100	0.87	0.125	0.50	0.96	0.42	0.12	0.54	0.96
3	12	12	15.0	90	0.83	0.17	0.50	0.95	0.41	0.16	0.57	0.98
4	14	14	17.5	75	0.71	0.29	0.51	0.92	0.36	0.27	0.63	0.97
5	18	14.3	19.5	73	0.68	0.32	0.58	0.92	0.36	0.30	0.66	1.02
6	18	18	22.5	60	0.43	0.57	0.63	0.90	0.27	0.51	0.78	1.05

A similar approximation is derivable for b^*_{sf}:

$$b^*_{sf}(x_{g2},x_{f2})=\frac{1}{N_2L_2}\int_{S2}xf\langle x\rangle dx\int_{S2}b_c(x,x')f\langle x'\rangle dx', \quad (31)$$

$$b^*_{sf}(x_{g2},x_{f2})\approx b_c(x_{g2},x_{f2}), \quad (32)$$

but the limits to this approximation have not yet been checked.

Having achieved a basic parameterization for each collection mode separately, we may superimpose the respective equations to gain a combined parameterization:

$$\frac{1}{x_{g2}}\frac{dx_{g2}}{dt}\bigg|_{c+s}=b^*_{cg}L_1+b^*_{sg}L_2, \quad (33)$$

$$\frac{1}{x_{f2}}\frac{dx_{f2}}{dt}\bigg|_{c+s}=b^*_{cf}L_1+b^*_{sf}L_2. \quad (34)$$

In order to explain the spectrum development shown in Part II, we define a total $b_g(x_g)$ to account for the growth of the x_g of the combined $S1$ and $S2$ spectrum:

$$\frac{1}{x_g}\frac{dx_g}{dt}\bigg|_{c+s}=b_g(x_g)L. \quad (35)$$

As shown in Part III,

$$b_g=(b^*_{cf}+b^*_{sg})(L_1/L)+b^*_{sg}(L_2/L). \quad (36)$$

Using (27), (28) and (36) we write (35) and (33) as

$$\frac{1}{x_g}\frac{dx_g}{dt}\bigg|_{c+s}=2b_cL_1+b^*_{sg}L_2, \quad (37)$$

$$\frac{1}{x_{g2}}\frac{dx_{g2}}{dt}\bigg|_{c+s}=b_cL_1+b^*_{sg}L_2. \quad (38)$$

Once r_g is beyond 50 μm, rates of growth are nearly the same because $b^*_{sg}\approx 2b_c$, in which case, according to (37), the growth rate of r_g will not be highly dependent on the relative values of L_1 and L_2.

It is of interest in this regard to calculate the growth rates for both r_{g2} and r_g for Figs. 1–6 of Part II at the moment $r_g = 50$ μm. The data are shown in Table I. The b_c and b^*_{sg} values are taken from Fig. 1. The r_{g2} values are estimated from the figures, and the L_2 are calculated from this estimate. It can be shown that the final answer is rather insensitive to error in estimating r_{g2}.

Table 1 shows that the growth rate of r_{g2} is much greater for those spectra with steeper $S2$ slopes and larger L_2. The values of b^*_{sg} are nearly the same in all cases, while the values of b_c increase with larger r_{f1}. It is easily seen that the dominating factor is L_2. Its effect is partially masked in the growth rates of the r_g's, where twice the value of L_1b_c is contributed. The r_g growth rates only gradually increase with r_b to give approximately equal sloped lines in Fig. 7, Part II. We conclude in either case, however, that the rapid achievement of high L_2 is the most important single factor in obtaining a fast growth rate by stochastic collection.

As a final demonstration of the importance of this effect, we show the development of several spectra where autoconversion is unimportant but accretion and self-collection are. Fig. 2 shows several initial spectra with various $S2$ and the same $S1$ with the total L adjusted to 1 gm m^{-3}. Fig. 3 shows the development of each case at $t=0$, 10 and 20 min.

We see that the two upper displays began with too large an r_{g2} and subsequently did not have b_c large enough to gather very much water from L_1. The two middle displays show that a small amount of water added near $r_{f2}=50$ μm accumulates L_1 rapidly and thereby increases L_2 so that self-collection can proceed at a rapid rate. The result is far more water on large drops in a shorter time than the first two instances could provide. The lower displays which began with $r_{f2}=20$ μm are at the end only some 8 min behind the middle two experiments.

We conclude that a proper recognition of the feedback between L_2 and r_{g2} is fundamental to parameterized reasoning of precipitation development. The behavior in Fig. 3 can be very closely predicted by the parameterizations in (37) and (38).

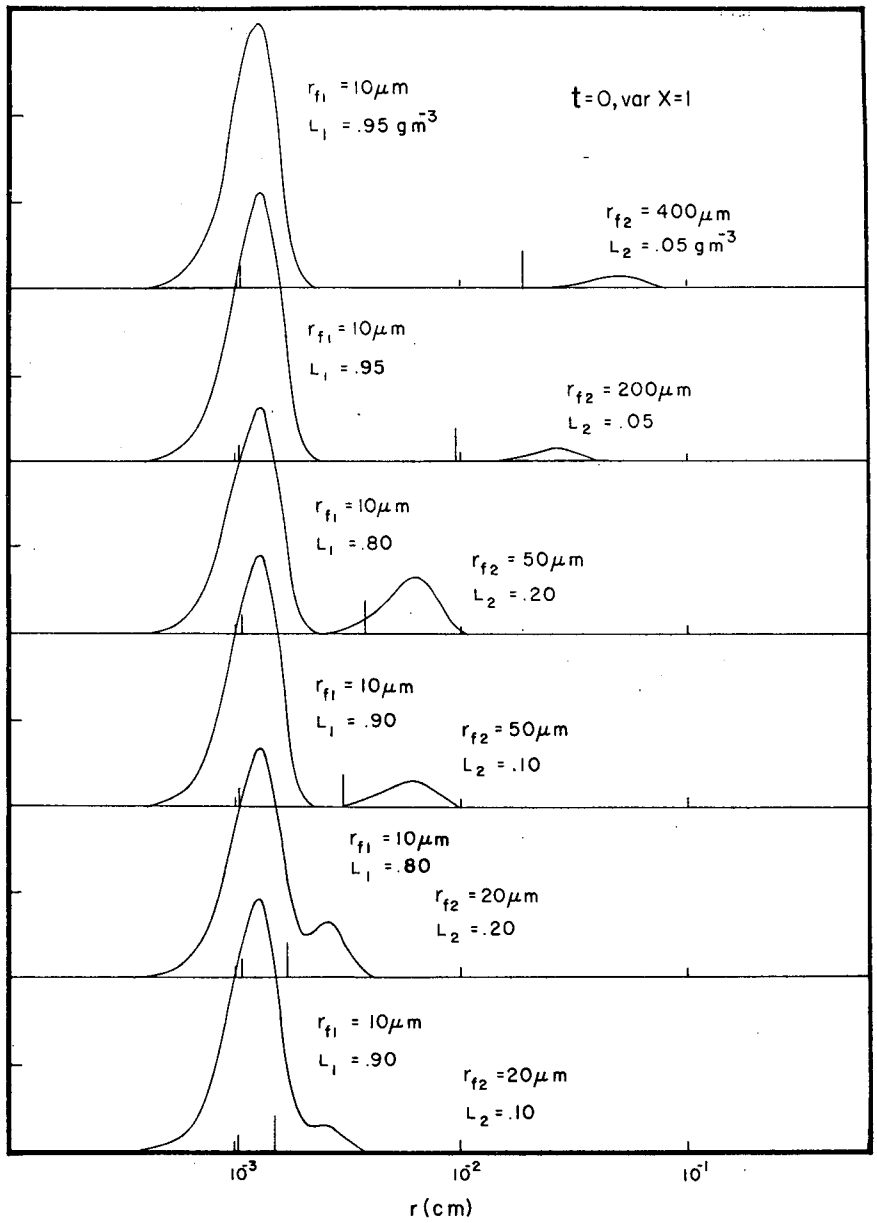

FIG. 2. Various initial distributions of $S2$ added to an initial spectrum with $r_{f1}=10^{-3}$, var $x=1$, total $L=10^{-6}$.

4. In retrospect

The first general parameterization of collection seems to have been that of Kessler (1969). He postulated a cloud model which consists of two size categories of drops: cloud droplets with insignificant fallspeeds, and hydrometeors; and used the terms autoconversion and accretion to describe the two primary mechanisms of drop growth as he perceived it.

It is interesting to note that we did not set out to put our collection parameterizations in terms of cloud water, hydrometeor water, autoconversion and accretion. We tried every other way we could think of, but the results of our calculations kept telling us to break spectrum at $r_g=50$ μm, and once we did, the pieces began to fall into place.

For convenience we will summarize the essential ingredients of Kessler's and our parameterization forms of hydrometeor collection. In our notation the Kessler method is

$$\frac{1}{L_2}\frac{dL_2}{dt}=K_2L_1L_2^{-1/8}, \tag{39a}$$

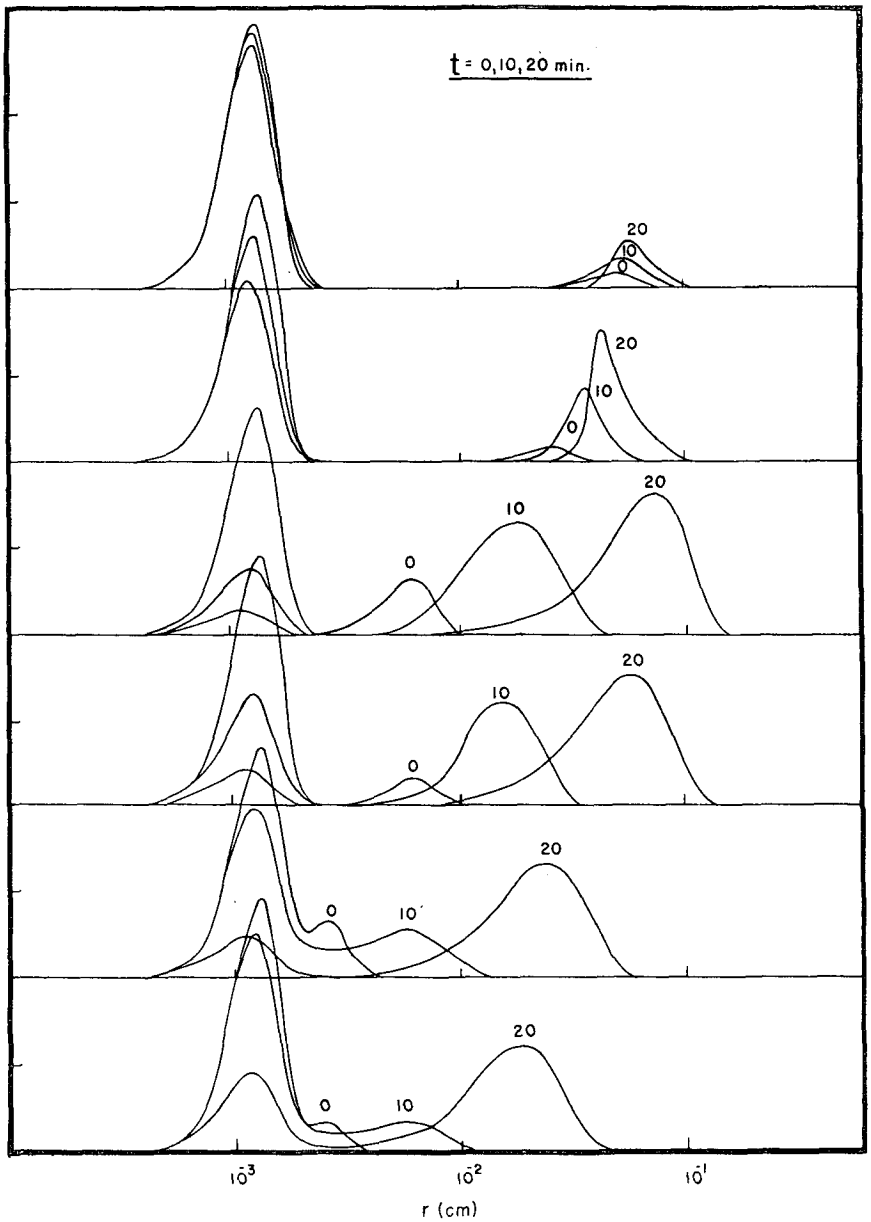

FIG. 3. The values of the spectra of Fig. 1 at 10-min intervals.

$$\frac{1}{D_0}\frac{dD_0}{dt}=\frac{1}{4}\frac{1}{L_2}\frac{dL_2}{dt}, \tag{39b}$$

$$\frac{1}{Z}\frac{dZ}{dt}=\frac{7}{4}\frac{1}{L_2}\frac{dL_2}{dt}, \tag{39c}$$

where K_2 is a constant, D_0 the median volume diameter, and Eq. (39b) results from the required fit to the Marshall-Palmer spectrum.

The method of parameterization that results from the present analysis is

$$\frac{1}{L_2}\frac{dL_2}{dt}=b^*_{cf}L_1, \tag{40a}$$

$$\frac{1}{x_{f2}}\frac{dx_{f2}}{dt}=b^*_{cf}L_1+b^*_{sf}L_2, \tag{40b}$$

$$\frac{1}{x_{g2}}\frac{dx_{g2}}{dt}=b^*_{cg}L_1+b^*_{sg}L_2, \tag{40c}$$

$$\frac{1}{Z}\frac{dZ}{dt}=\frac{1}{L_2}\frac{dL_2}{dt}+\frac{1}{x_{g2}}\frac{dx_{g2}}{dt}, \tag{40d}$$

where the first term on the right-hand side is due to accretion and the second to self-collection. The rate

coefficients are as follows:

$$b_{cf}^{*}=\frac{1}{L_2}\int_{S2} b_c(x_2,x_1)x_2 f\langle x_2\rangle dx_2 \approx b_c(x_{g2},x_{f1}) \quad (41a)$$

$$b_{cg}^{*}=\frac{1}{L_2}\int_{S2} b_c(x_2,x_1)\left(\frac{2x_2}{x_{g2}}-1\right)x_2 f\langle x_2\rangle dx_2 \approx b_c(x_{g2},x_{f1}) \quad (41b)$$

$$b_{sf}^{*}=\frac{x_{f2}}{L_2^{2}}\int_{S2} x_2 f\langle x_2\rangle dx_2\int_{S2} b_c(x_2,x_2')f\langle x_2'\rangle dx_2' \approx b_c(x_{g2},x_{f2}) \quad (41c)$$

$$b_{sg}^{*}=\frac{2}{x_g L_2^{2}}\int_{S2} x_2^{2} f\langle x_2\rangle dx_2\int_{S2} b_c(x_2,x_2')x_2' f\langle x_2'\rangle dx_2' \approx 2b_c(3.4x_{g2},x_{g2}) \quad (41d),$$

$$b_c(r_2,r_1)=\frac{3}{4\rho}\left(\frac{r_2^{2}}{r_2^{3}+r_1^{3}}\right)\Delta v(r_2,r_1)Y_c^{2}(r_2,r_1). \quad (42)$$

By way of comparison we notice that b_{cf}^{*} in (40a) replaces $K_2L_2^{-1/8}$ in (39a) but this difference is unimportant since both quantities are calculated from the same accretion equation. Comparing the accretion portion of (40b) with (40a) we see that

$$\frac{1}{x_{f2}}\frac{dx_{f2}}{dt}\bigg|_c=\frac{1}{L_2}\frac{dL_2}{dt}, \quad (43a)$$

$$\frac{1}{r_{f2}}\frac{dr_{f2}}{dt}\bigg|_c=\frac{1}{3}\frac{1}{L_2}\frac{dL_2}{dt}. \quad (43b)$$

Comparing (43b) to (39b) we see that D_0 is constrained to grow more slowly than r_{f2} by accretion. This, however, could well better account for the effect of drop breakup which is necessary to produce the Marshall-Palmer spectrum and which must yet be added to the present parameterization. The key difference between the two methods is in the self-collection. Absent in the older method, this process serves in the newer method to free the dependence of the mean mass (x_{f2}, x_{g2} or D_0^3) on the total mass (L_2), and opens the parameterization to the inclusion of important microphysical feedback effects. Two spectral moments are used which together contain information about the variance of the spectrum.

The radar reflectivity is readily seen to be the same equation in both cases. The distinction in the new parameterization lies in the independent treatment of added water mass due to accretion and increased predominant mass due to self collection.

5. Conclusion

The spreading or narrowing of a droplet spectrum undergoing collection is dependent upon the kernel in the region of interest and the mode of collection that is in effect. The accretion process produces no spreading for rapidly increasing kernels, a slow approach to var $x=1$ for a moderately increasing kernel, and progressive narrowing for a constant kernel.

The stochastic mode is a necessary but not a sufficient condition for rapid spreading of the spectrum. It is also necessary that the collection kernel increase sufficiently rapidly with drop size. It seems more correct to say that this kernel increase is the cause of spectrum spreading and stochastic collection is the mode through which the kernel operates. In the stochastic mode a rapidly increasing kernel produces rapid spreading, an intermediate kernel produces moderate spreading, and a constant kernel drives the shape toward var $x=1$.

A new parameterization of cloud particle growth has been described which superimposes the effects of accretion and self-collection and thereby allows water mass and spectral moments to change independent of one another. Drop breakup is not included at this stage. The parameterization can readily be extended to include the ice phase and will include feedback processes essential to the modelling and explanation of cloud particle growth.

Growth rates due to accretion are proportional to cloud water content; those of self-collection, to large hydrometeor water content. Therefore, the rapid accumulation of large hydrometeor water content will do more toward the generation of large hydrometeors than the maintenance of high cloud water content. Since the shape of the large hydrometeor distribution is dependent upon the relative magnitudes of accretion and self-collection (as well as breakup which is neglected here), this shape is therefore a clue to the physical processes operating within the cloud.

APPENDIX

List of Symbols

b	total rate coefficient, accretion plus self-collection
b_c	rate coefficient for accretion only
b_s	rate coefficient for self-collection only
f	number density function
g	mass density function
L	liquid water content
N	total number density
r	droplet radius
r_f	radius corresponding to $x_f=L/N$
r_g	radius corresponding to $x_g=Z/L$
$S1$	the small hydrometeor or "cloud water" portion of the spectrum
$S2$	the large hydrometeor portion of the spectrum
V	collection kernel
var x	relative variance with respect to mass $[=(x_g/x_f)-1]$

x droplet mass
x_f mean mass of the number density function
x_g mean mass of the mass density function
Z spectral radar reflectivity, the second mass moment of the number density function.

REFERENCES

Berry, E. X, 1967: Cloud droplet by collection. *J. Atmos. Sci.*, **24**, 688–701.

——, and R. L. Reinhardt, 1974a: An analysis of cloud drop growth by collection: Part I. Double distributions. *J. Atmos. Sci.*, **31**, 1814–1824.

—— and ——, 1974b: An analysis of cloud drop growth by collection: Part II. Single initial distributions. *J. Atmos. Sci.*, **31**, 1825–1831.

—— and ——, 1974c: An analysis of cloud drop growth by collection: Part III. Accretion and self-collection, *J. Atmos. Sci.*, **31**, 2118–2126.

Kessler, E., 1969: On the distribution and continuity of water substance in atmospheric circulations. *Meteor. Monogr.*, **10**, No. 32, 84 pp.